Cobalt-Based Fischer–Tropsch Activity and Selectivity as a Function of Crystallite Size and Water Partial Pressure

ARTICLE *in* ACS CATALYSIS · NOVEMBER 2014

Impact Factor: 9.31 · DOI: 10.1021/cs500936t

4 AUTHORS, INCLUDING:

Nico Fischer
University of Cape Town
12 PUBLICATIONS **90** CITATIONS
SEE PROFILE

M. Claeys
University of Cape Town
68 PUBLICATIONS **1,409** CITATIONS
SEE PROFILE

ACS Catalysis

Research Article

pubs.acs.org/acscatalysis

Cobalt-Based Fischer–Tropsch Activity and Selectivity as a Function of Crystallite Size and Water Partial Pressure

N. Fischer, B. Clapham, T. Feltes, and M. Claeys*

Centre for Catalysis Research and c*change (DST-NRF Centre of Excellence in Catalysis), Department of Chemical Engineering, University of Cape Town, Cape Town 7701, South Africa

ABSTRACT: Using well-defined supported cobalt nanocrystallites in a novel in situ sample presentation device for laboratory X-ray diffractometers, we investigated the extensively studied structure sensitivity of Fischer–Tropsch (FT) catalysts under simulated high conversion conditions, that is, at high water to synthesis gas ratios. This study has to be regarded as a further small step toward a full understanding of the various processes governing FT activity and selectivity. We were able to show, for two different crystallite sizes, that water has an overall enhancing effect on carbon monoxide conversion and surface specific turnover frequency on metallic surfaces and improves the overall product selectivity with a decrease of methane selectivity. For small crystallites oxidation was observed at elevated water partial pressures, which caused a decrease of activity. The selectivity to the undesired product methane is suppressed in favor of chain growth. This influence on the selectivity might originate from water-induced changes on the active sites responsible for chain growth or by an inhibiting effect of water on methanation sites. Due to a stronger effect of water on smaller crystallites, the impact on the methane selectivity reverses previously described trends of increasing methane selectivity with decreasing crystallite size. Secondary olefin reactions, clearly more pronounced on smaller crystallites and under "dry" conditions, are severely suppressed via the addition of water, resulting in a pseudo structure insensitivity of this class of reactions.

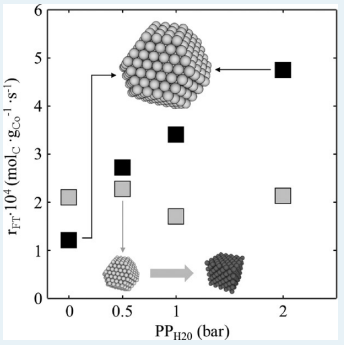

KEYWORDS: *Fischer–Tropsch synthesis, co-feeding of water, cobalt nanoparticles, activity, selectivity*

1. INTRODUCTION

To design the most active and selective catalyst at the lowest possible raw-material cost is the most important target of all catalyst-producing companies.[1] For metal-based heterogeneous catalysts, the main cost factor is usually the active metal phase. To minimize its content without losing the desired activity, metals are often deposited as small crystallites, down to the single-digit nanometer range, on an inert carrier material so as to maximize the mass specific surface area. Some reaction mechanisms, however, have been reported to require a certain arrangement of surface atoms, a so termed minimum required ensemble, to provide the desired performance.[2] In the absence of these ensembles the catalyst may show no or undesired activity/selectivity. Two prominent reactions showing such a catalyst structure sensitivity are the CO oxidation over gold catalysts[3] and the here-studied Fischer–Tropsch (FT) synthesis.[4] The majority of the latter studies were carried out under mild reaction conditions to avoid crystallite growth of the employed model catalyst systems due to reaction temperature and product water. The study presented here has to be regarded as a first step to elucidate the crystallite size effect under industrial conditions, focusing solely on the intrinsic crystallite size effect. Variables such as the presence of hydrocarbons, in both gas and liquid phases, and the CO_2 partial pressure as well as the presence of product water will have to be added piece by piece to build a concise understanding of the different effects and their interplay at work. Water has been reported to enhance sintering at high concentrations.[5] However, water has also been reported to influence the activity[6] as well as selectivity[6d−f,7] of a Fischer–Tropsch catalyst. Therefore, some of the previously observed activity and selectivity trends reported for different crystallite sizes under "dry" conditions might not hold under realistic industrial conversion conditions. It is desired to test the effect of water on the catalytic performance with simulated conversions at and beyond currently industrially employed conditions. Although not relevant today, one has to be aware that it is of great interest to industry to intensify the cobalt-based FT process by increasing the per-pass conversion. Currently set conversion is limited mainly through the high water partial pressures, which are detrimental to the catalyst's lifetime and, as a result, render the current process uneconomical.[8] To achieve this goal it is imperative to exactly understand the effect of water on stability[9] as well as on the activity and selectivity of the cobalt catalyst system, especially as currently used rate equations for cobalt-based FT to not contain a term accounting for the water partial pressure in contrast to iron-based FT catalysts.[8,10]

In this study we combine the approach to use well-defined supported cobalt crystallites as model catalyst systems and first

Received: July 1, 2014
Revised: November 9, 2014

   dx.doi.org/10.1021/cs500936t | *ACS Catal.* 2015, 5, 113−121

Table 1. Reverse Micelle Composition for the Preparation of the Studied Cobalt Model Catalysts

	mass (g)					
catalyst	*n*-hexane	Berol 050	water	$Co(NO_3)_2{\cdot}6H_2O$	$NH_4(OH)$ solution (mL)	ω^a
A	999.90	136.65	52.76	5.12	5.40	0.4
B	2000.01	273.59	54.24	1.32	1.35	0.2

[a]Molar water to surfactant ratio.

expose them to mild Fischer–Tropsch conditions, that is, low temperature and high space velocity resulting in low conversion. In addition, we co-feed defined amounts of water to the synthesis gas mixture simulating high conversion conditions without generating concentration gradients over the catalyst bed. To correlate the observed conversion and selectivities with the actual working catalyst system, all experiments were conducted in an in-house developed in situ X-ray diffraction cell assembly.[9,11]

2. EXPERIMENTAL SECTION

2.1. Catalyst Preparation. Two alumina-supported cobalt model catalysts with different cobalt crystallite sizes were prepared using a reverse micelle method as previously described,[12] with the exact compositions given in Table 1. In short, an aqueous solution of cobalt nitrate hexahydrate (Sigma-Aldrich) was added to a mixture of *n*-hexane (Kimix, RSA) and the nonionic surfactant Berol 050 (pentaethylene glycol dodecyl ether, AkzoNobel), forming a stable reverse micelle or microemulsion. Aqueous ammonium hydroxide solution (25 wt %, Sigma-Aldrich) was added dropwise to form cobalt hydroxide, entrapped in the reverse micelle structure. The latter is destabilized via the addition of acetone. Precipitated hydroxide is collected, washed in acetone, dried in air at 120 °C, and subsequently calcined at 200 °C, yielding nanocrystalline Co_3O_4. The desired amount of the cobalt oxide is resuspended in water under ultrasonication, mixed with the alumina support (Al_2O_3, Puralox SCCa 5-150 series, S_{BET} = 162 m^2/g, V_{pore} = 0.47 cm^3/g, d_{pore} = 11.5 nm, $d_{particle}$ = 150–200 μm; Sasol, Germany), and dried under reduced pressure in a rotary evaporator. Crystallite size variation was achieved via variation of the composition of the reverse micelle systems used, the higher water to surfactant ratios and the higher cobalt salt concentrations yielding the larger crystallites (see also below).

2.2. Catalyst Characterization and Testing. Transmission electron microscopy (TEM, LEO 912 operated at 120 kV) analysis of the unsupported Co_3O_4 crystallites was used to determine the crystallite size distributions obtained. The targeted loading of cobalt (approximately 7 wt %) on the alumina support was confirmed by means of atomic absorption spectroscopy (AAS, Varian SpectraAA 110).

The identification of the crystallite phases and corresponding sizes of the model catalysts as well as their activity and selectivity under Fischer–Tropsch conditions was performed using an in-house developed in situ XRD cell attached to a conventional X-ray diffractometer (Bruker D8 Advance). Quantitative data regarding size and concentration were obtained from Rietveld refinement using Topas 4.2. The in situ XRD cell, which employs a capillary reactor (loaded with 10.3 mg of catalyst A and 13.7 mg of catalyst B, respectively) and a thermocouple placed inside the catalyst bed for accurate temperature control, is described in detail elsewhere.[9,11] Prior to the exposure of the model catalysts to Fischer–Tropsch conditions, the cobalt oxide phase (Co_3O_4) was reduced in a hydrogen gas flow of 80 $mL_{NPT}{\cdot}min^{-1}{\cdot}g^{-1}$ at atmospheric pressure at 450 °C for 6 h using a ramping rate of 1 °C·min^{-1}. The reduced catalyst was cooled under hydrogen to 220 °C and exposed to a flow of the synthesis gas mixture consisting of hydrogen, carbon monoxide, and argon in a ratio of 6:3:1 at 80 $mL_{NPT}{\cdot}min^{-1}{\cdot}g^{-1}$. The synthesis gas partial pressure was maintained throughout the experiments at 1 bar. In conjunction with the high space velocity, the resulting low conversions (<10% CO conversion) guarantee a negligible partial pressure of product water and the absence of significant reactant concentration profiles along the catalyst bed. Higher conversions were simulated via the stepwise addition of water vapor via a saturator, the temperature of which determined the resulting water vapor or partial pressures, respectively (see Table 2). The total pressure was increased according to the amount of water fed, so that the water partial pressure was the only parameter varied. Each condition was maintained for 6 h to allow the system to stabilize. It is important to note that the thermodynamic feasibility of the oxidation of small crystallites is determined by the ratio of water to hydrogen and not total pressure levels.[13] The approach taken in this study, where the syngas pressure was kept constant and the ratio of water to syngas or hydrogen (see Table 2), respectively, was varied systematically, therefore allows us to study the effect of conversion at a syngas pressure level of 1 bar. The reactor outlet gas was directly analyzed with an online GC-TCD (Varian CP4900). Additionally gas samples were taken with the ampule method[14] and analyzed in an offline FID (Varian CP3900). No kinetic data were recorded at water partial pressures of 3 bar. Under these conditions only possible phase changes were studied with the X-ray diffractometer.

Table 2. Water Partial Pressures (PP_{H2O}) and Corresponding Simulated Conversions

PP_{H2O} (bar)	PP_{H2O}/PP_{H2} (bar/bar)	$T_{saturator}$ (°C)	$X_{CO,simulated}$ (%)	$P_{reactor}$ (bar)
0	0	n/a	n/a	1.0
0.5	0.75	82	63	1.5
1	1.5	100	77	2
2	3	120	87	3
3	4.5	134	91	4

Both model catalyst were studied with TEM in the oxidic unsupported and in the supported stage before and after reduction (catalyst was cooled to room temperature and passivated in a flow of 1% O_2 in N_2). After the experiments, the spent catalysts were again characterized with TEM.

3. RESULTS AND DISCUSSION

The cobalt oxide catalyst precursor was characterized with standard offline techniques such as TEM and AAS. The reduction and all following reaction steps were analyzed in situ using X-ray diffraction. Reactor outlet gases were identified with

dx.doi.org/10.1021/cs500936t | ACS Catal. 2015, 5, 113–121

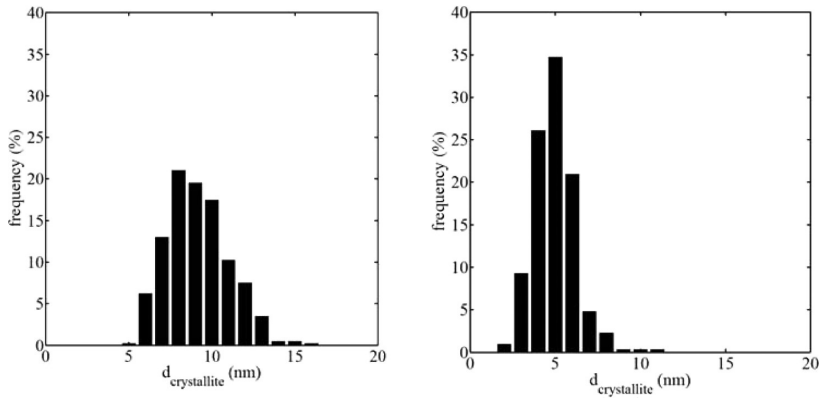

Figure 1. Crystallite size distribution obtained from the analysis of more than 300 unsupported Co_3O_4 crystallites of catalysts A (left) and B (right) in TEM micrographs. Size distributions are number based.

gas chromatographic techniques. After passivation, the spent catalyst was further analyzed with TEM to confirm trends observed in the in situ XRD studies.

3.1. Model Catalyst System. The results of XRD characterization confirmed the formation of a pure cobalt oxide spinel phase, Co_3O_4, in the unsupported product of the catalyst calcination. The crystallite sizes obtained via Rietveld refinement of the XRD data as well as from the analysis of TEM micrographs are in good agreement (see Figure 1 and Table 3).

Table 3. Characterization Results of the Oxidic Catalyst Precursor

			Co_3O_4 crystallite size		
catalyst	ω^a	$Co(NO_3)_2{\cdot}6H_2O$ concn (mol/L)	XRD[b] (nm)	TEM[c] (nm)	loading ASS (wt %)
A	0.4	0.32	11.1	10.3 ± 1.9	6.4
B	0.2	0.08	6.7	6.1 ± 1.4	4.0

[a]Molar water to surfactant ratio. [b]Crystallite sizes (volume-based average) determined from XRD analyses; calculated using Rietveld refinement. [c]Crystallite sizes (average and standard deviation) determined from TEM analyses; note that the sizes given are volume based (recalculated from number-based distributions) to allow for direct comparison with XRD data.

Indeed, the variations in the reverse micelle composition result in two distinctly different size fractions, namely, 10−11 nm for catalyst A and 6−7 nm for catalyst B. Both catalyst precursors display a fairly narrow particle size distribution (see Figure 1 and standard deviations in Table 3), making them ideally suitable for model catalyst studies aiming at unravelling size dependencies/effects. With AAS the final loading of the Co_3O_4 crystallites on the alumina support was determined as being 6.4 and 4.0 wt % cobalt for catalysts A and B, respectively. The cobalt loading chosen in the present study is significantly higher than previously realized with the reported preparation method[4a,12] to allow for better signal-to-noise ratio in the in situ XRD measurements. As the prepared cobalt oxide spinel nanocrystallites are dispersed on the alumina support by ultrasonication, that is, in the absence of anchoring chemical bonds which would lead to metal support interactions,[15] a higher loading results in a decreased average distance between single crystallites, higher probability of cluster formation, and therefore higher probability of crystallite growth during a thermal treatment such as reduction. These risks are accepted in the context of this study as long as after reduction two model catalyst systems with distinct sizes of metallic nanoparticles are obtained. TEM analyses of the supported model catalyst show a slight agglomeration of the Co_3O_4 crystallites (see Figure 2, top). This is more pronounced in the case of catalyst A. Possible reasons for this difference are the higher loading and the larger average crystallite size (i.e., larger than the pore size of the support, 11.5 nm), rendering the Co_3O_4 crystallites more difficult to resuspend under ultrasonication. After reduction at 450 °C in hydrogen (see section Catalyst Characterization and Testing for experimental details), TEM micrographs of catalyst A show a severe increase in crystallite size (see Figure 2, bottom) to an average of 21.3 ± 5.6 nm, whereas catalyst B retains its average crystallite size (5.6 ± 1.3 nm).

3.2. Fischer−Tropsch Synthesis. *3.2.1. Phase Stability and Fischer−Tropsch Activity.* As previously reported[9] catalyst A does not fully reduce under the applied conditions and a residual content of Co^{2+} oxide is still detectable, whereas with catalyst B full reduction was obtained (see Figure 3 for crystallite sizes obtained during reduction and reaction work). The only measurable phase of metallic cobalt was the face-centered cubic (fcc) modification. Average crystallite sizes in the reduction process from Co_3O_4 via CoO to fcc-Co should, in the absence of any secondary effects, decrease by approximately 25% due to the loss of oxygen.[16] In the case of catalyst A, a crystallite size increase from the oxide precursor to the metallic phase was measured (from 11.1 to 20.4 nm). Although the sizing of the latter phase is affected by a relatively large error resulting from overlapping peaks of the diffraction pattern of the metallic phase and the support material, a crystallite growth process, that is, sintering, is evident. For catalyst B the expected decrease in crystallite size (from 6.7 to 4 nm), clouded as to its absolute extent by the mentioned uncertainties, is observed. Possibly, small crystallites undergo a more intimate contact with the support, forming anchoring sites in pores of the support (average pore diameter = 11.3 nm) and hence reducing the risk of crystallite growth. The larger crystallites of catalyst A, on the other hand, might be too large for the pores of the support and therefore more susceptible for sintering. A similar effect was previously observed by comparing different variations of the reverse micelle approach to prepare alumina-supported cobalt model catalysts. When larger particles are deposited (diameter influenced through surfactant layer present around a $Co(OH)_2$ precipitate compared to calcined Co_3O_4), the effect of sintering was more pronounced.[15] Upon exposure to synthesis gas and upon the addition of elevated partial pressures of water, to simulate higher conversions, the

dx.doi.org/10.1021/cs500936t | ACS Catal. 2015, 5, 113−121

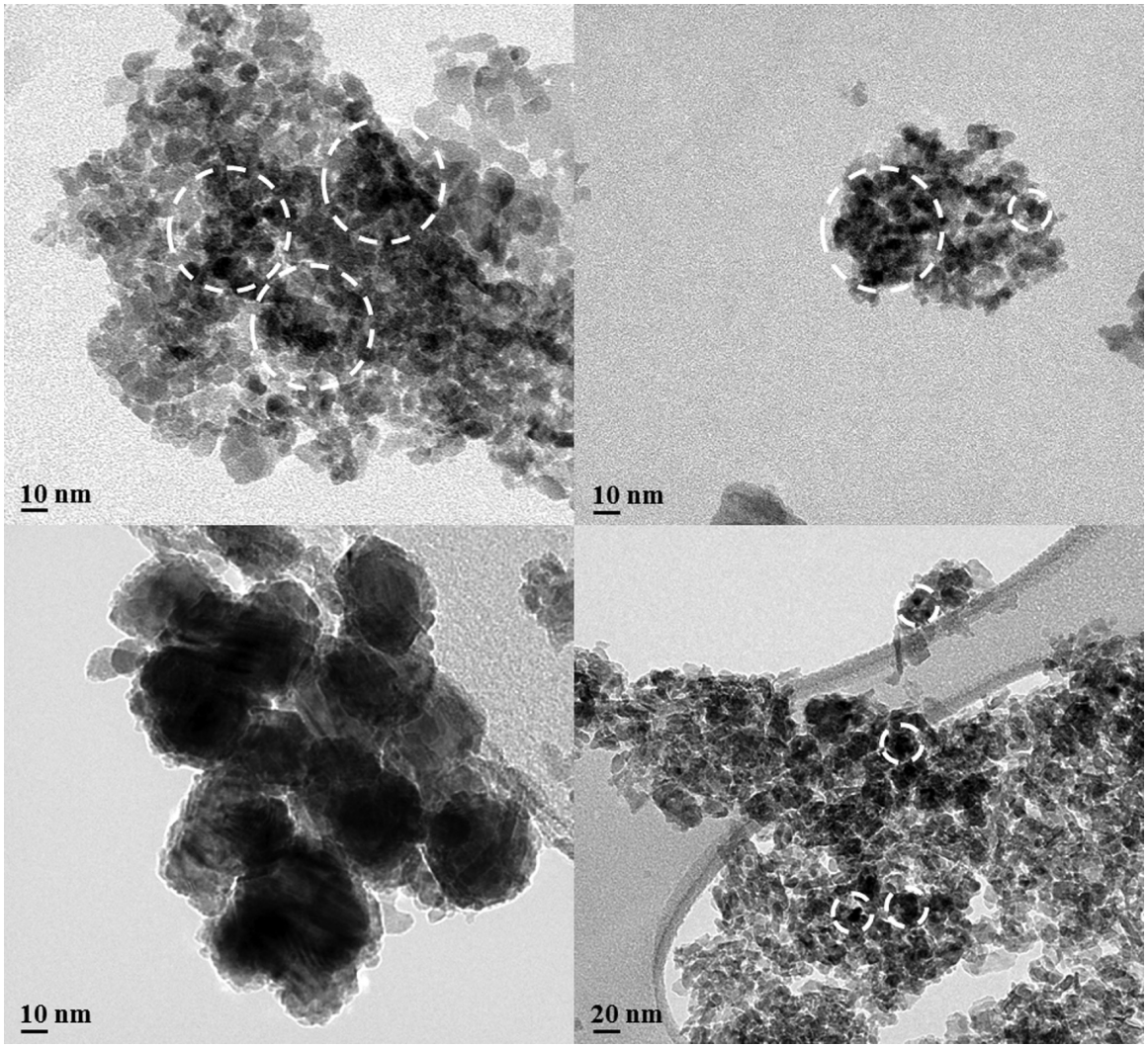

Figure 2. TEM micrographs of the supported catalyst A (left) and catalyst B (right) in the oxidic (top) and reduced (bottom) state. Identified areas of crystallite agglomeration and single crystallites are indicated.

crystallite sizes and phases present in catalyst A do not change significantly. In contrast, catalyst B undergoes partial oxidation upon the addition of 0.5 bar PP_{H2O} (70% of metallic cobalt oxidized to CoO) and full oxidation to Co^{2+} oxide at higher water contents. The observed size effect has been previously reported by us in detail[9] and is in agreement with theoretical studies.[13] Previous studies on crystallite size dependencies have hypothesized that oxidation of cobalt nanocrystallites might occur[13,17] but that under industrially relevant conditions the water partial pressure is too low.[5,17b] Work by the Davis group[18] showed that cobalt on silica and alumina catalysts is influenced by the addition of water. They concluded the formation of cobalt oxide species upon the initial exposure to elevated water pressures, a species that upon prolonged exposure can either undergo sintering and reduction or form cobalt aluminates. Interestingly, in the present study, whereas CoO is the only detectable X-ray visible phase, catalyst B still shows significant Fischer–Tropsch activity under all studied water partial pressures (see Figure 4). As CoO is not active for the hydrogenation of carbon monoxide and subsequent chain growth, very small crystallites, thin layers or amorphous metallic cobalt, or very small concentrations of larger crystallites, all being below the sensitivity limit of laboratory X-ray diffraction under the presented experimental conditions, need to be present to explain the observed activity. Indeed, in the complementary study focusing on the oxidation potential of water,[9] magnetic measurements of a very similar model catalyst system showed a severe loss in magnetization due to the oxidation of Co to CoO, however retaining approximately a fourth of the initial magnetization, that is, reduced cobalt species, after 5 h under a simulated CO conversion of 66.7%. The exact position and structure of the metallic cobalt fraction could not be determined.

Under "dry" conditions, the overall CO conversion is within 1.2% the same for both catalyst systems. Due to the differences in cobalt loading (see Table 3) as well as catalyst loading in the capillary cell, this translates to a by nearly 2-fold higher cobalt mass specific reaction rate for catalyst B (see Figure 4, left). This observation is in line with previous studies reporting an ideal crystallite size regarding the mass specific activity for cobalt-based Fischer–Tropsch synthesis of 6–8 nm.[4a,19] Upon the addition of water vapor to the reactor inlet gas, the Fischer–Tropsch rate increases by a factor of 4 for catalyst A while remaining relatively constant for catalyst B. The difference in the observed effects of water on the mass specific activity can be correlated to the different changes in the

dx.doi.org/10.1021/cs500936t | ACS Catal. 2015, 5, 113–121

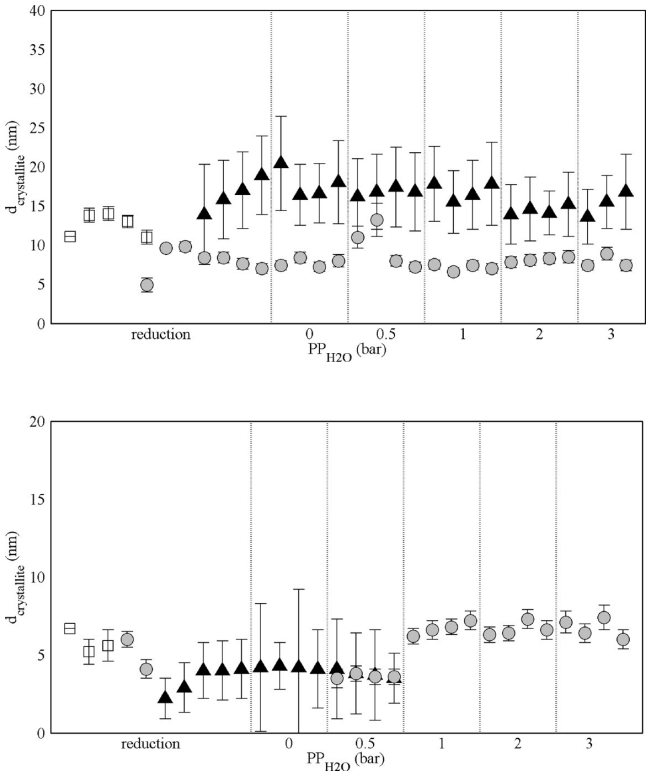

Figure 3. Crystallite sizes of Co_3O_4 (open squares), CoO (gray circles), and fcc-Co (black triangles) for catalysts A (top) and B (bottom) as a function of reaction conditions. Values determined by Rietveld refinement in TOPAS 4.2. Reproduced with permission from ref 9. Copyright 2014 Wiley-VCH.

oxidation states of the model catalysts. Catalyst A retains its predominantly metallic character, that is, phase composition, as well as crystallite size independent of the elevated levels of water. The change in activity can therefore directly be correlated to the increased water partial pressures. In the case of catalyst B, the metallic content is reduced upon the introduction of 0.5 bar water vapor by 70% in favor of CoO. This severe loss in active phase content should result in a clear loss in activity. The observed stable activity, seemingly independent of water partial pressures, can therefore be identified as the sum of two opposing effects: a decrease in active material due to the oxidizing effects of co-fed water and an activating effect of water on the remaining active sites as can be observed for catalyst A. The extent of the latter cannot be quantified in this study but is hypothesized to be crystallite size dependent. Previously the addition of water to an alumina-supported cobalt Fischer–Tropsch catalyst has been reported to cause the catalyst to deactivate, which was correlated to the oxidizing potential of water or a reversible competitive adsorption on the catalytic surface.[18a,b,d,20] In contrast, other studies on silica and titania as well as alumina-supported cobalt and ruthenium catalysts report an enhanced Fischer–Tropsch activity upon the addition of water.[6,18c] The observed increase in activity was explained by a facilitated CO dissociation step by coadsorbed water.[6a] In addition, it was noted that an increase in water partial pressure would result in a decrease of surface carbon species, which have been considered to inhibit the Fischer–Tropsch reaction.[6d] Schulz et al. further noted that water could influence the elemental reaction steps affecting not only activity but also selectivity.[6e,f,7] Water has also been described as a hydrogen shuttle, further lowering the dissociation energy required for the hydrogen-assisted CO dissociation, a process that is believed to play a role in relatively unreactive surfaces such as terrace sites of cobalt crystallites[21] or in ruthenium surfaces.[22] For large cobalt crystallites, where the terrace sites constitute a higher percentage of the surface atoms, one would therefore expect a higher impact of co-fed water than on small crystallites where edge and kink sites dominate. In the present study this trend could not be confirmed as the smaller crystallites show a decreased stability against the oxidative pressure of water. Plotting the turnover frequency (TOF), that is, the number of moles of carbon monoxide converted per available surface cobalt atom and time (under the assumption of ideal cubooctahedric cobalt particles, as described in the literature,[23] and no unavailability of cobalt surface area due to the interface with the support material), shows 2- and 3.2-fold increases in activity for catalysts A and B, respectively (see Figure 4, right). Again, the proposed role of water as a hydrogen shuttle on terrace sites[21] could therefore not be confirmed under the present conditions due to two different superimposing effects. The lower TOF of catalyst B can be explained by the smaller crystallite size, and this has been reported extensively in the literature for cobalt-based catalysts[4a−c,f,24] and other FT active materials.[4e,25]

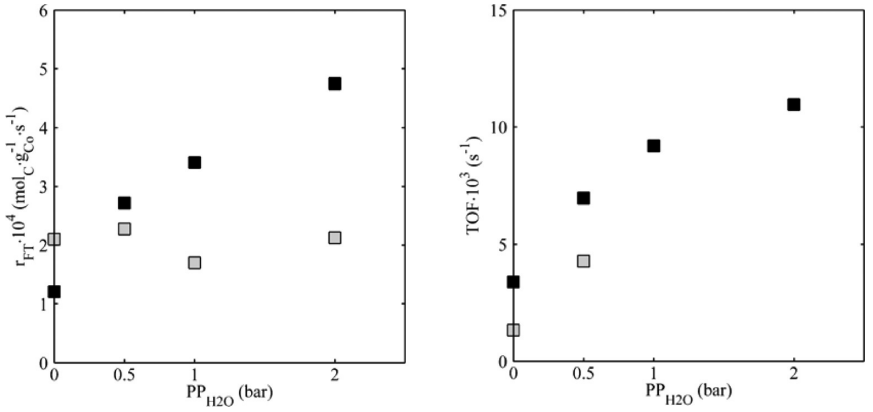

Figure 4. Rate of Fischer–Tropsch product formation per gram of cobalt (left) and turnover frequency (right) as a function of water partial pressure for catalyst A (black squares) and catalyst B (gray squares). Note that due to the absence of an XRD visible metallic cobalt phase for catalyst B above water partial pressures of 0.5 barn no turnover frequency could be calculated.

dx.doi.org/10.1021/cs500936t | ACS Catal. 2015, 5, 113−121

3.2.2. Chain Growth Probability and Product Selectivity. Upon the addition of water to the Fischer–Tropsch reaction conditions, the chain growth probabilities (calculated from the straight-chained hydrocarbon products with a carbon number from 3 to 6) for catalysts A and B increased 2-fold, with catalyst B, that is, the smaller cobalt crystallites, displaying a larger enhancement (see Figure 5). This general trend has been

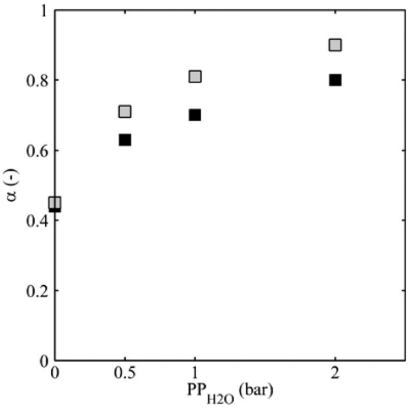

Figure 5. Chain growth probability α as a function of water partial pressure for catalyst A (black squares) and catalyst B (gray squares).

observed by other research groups[6a,b,e,f,7,17a,18c] and has been attributed to effects of water inhibiting product desorption.[7] Interlinked with the chain growth probability are the selectivities to the different product fractions, such as methane and the C_{5+} fraction (see Figure 6). Under "dry" conditions, both model catalysts show very similar selectivities to methane and higher hydrocarbons, irrespective of the cobalt crystallite size. Although this seems to be in contrast to previously reported increases in methane selectivity with decreasing crystallite size,[4a–c,f,25a,26] previous studies have shown that the extent of the size dependency of selectivities is a function of reaction conditions; that is, at milder conditions and lower conversions fewer differences in selectivity with crystallite size can be expected.[4a,d] Upon the addition of water, chain growth, that is, the insertion of C_1 species such as a methylene species[27] into a growing chain, is favored over the hydrogenation and desorption as methane.[6b,c,e,f,7,18c] As such, the selectivity to methane drops significantly with a simultaneous increase of the selectivity of the C_{5+} fraction (see Figure 6). Overall, the smaller crystallites in catalyst B show a higher degree of chain growth enhancement upon the addition of water vapor. This trend is so pronounced that under the effect of additional water partial pressure the smaller crystallites in catalyst B even outperform the larger crystallites with respect to low methane and high C_{5+} selectivity. This shows that the addition of a second activity and selectivity steering effect can revert previously identified intrinsic effects of the crystallite size in the absence of water.[4a–c,f,25a,26] Further studies, stepwise including additional variables such as the presence of liquid hydrocarbons, will be necessary to fully deconvolute contributions of these various effects on activity and selectivity observed under industrial conditions.

The two main classes of hydrocarbons formed in the Fischer–Tropsch synthesis are *n*-paraffins and α-olefins.[6e,28] In the absence of re-adsorption of olefins and subsequent hydrogenation or incorporation, a primary olefin selectivity of 70–90 mol % can be expected per carbon number.[28d,f,29] Carbon number dependent differences in olefin content have also been described. With ethylene being highly reactive and rapidly undergoing secondary reactions, it is detected in the Fischer–Tropsch product spectrum in lower quantities than expected from an ideal Anderson–Schulz–Flory distribution. Propene is therefore often the olefin found in the highest abundance per carbon number fraction as with increasing carbon numbers the tendency to undergo secondary reaction increases due to the changes in the carbon number dependent diffusion rates,[28e] solubility,[29b] and/or physisorption,[30] which result in longer contact times of the adsorbed olefin species on the catalytic surface and increased reactor residence times. Catalyst A shows, regardless of the reaction conditions, a relatively stable and primary olefin content in the total linear hydrocarbon fraction (see Figure 7, left). In comparison, the olefinic product with catalyst B clearly undergoes severe secondary reactions at "dry" conditions (see Figure 7, right). Upon the addition of water vapor secondary olefin reactions are inhibited and the product spectrum turns into a more primary composition. In a very comparable study by us with focus on the crystallite size dependency in the size range from approximately 2 to 11 nm,[4a] where the same model catalysts were used, no differences in the olefin content were observed. In our previous study a higher synthesis gas pressure of 9.9 bar was applied and a 10-fold higher Fischer–Tropsch product formation rate was observed, although also "dry" conditions with low conversions were applied. Possibly the resulting higher water partial pressure is already sufficient to suppress secondary

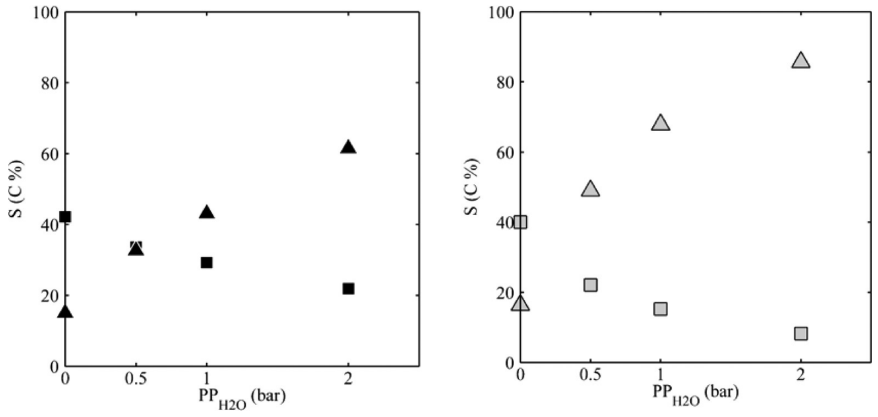

Figure 6. Methane (squares) and C_{5+} selectivities (triangles) as a function of water partial pressure for catalyst A (left) and catalyst B (right).

dx.doi.org/10.1021/cs500936t | ACS Catal. 2015, 5, 113–121

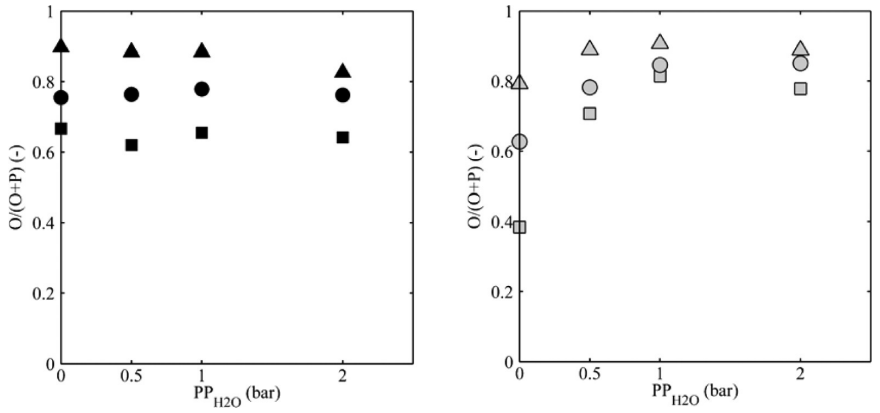

Figure 7. Fraction of olefin content in total linear hydrocarbon content for C_2 (squares), C_4 (triangles), and C_6 (circles) fractions as a function of water partial pressure for catalyst A (left) and catalyst B (right).

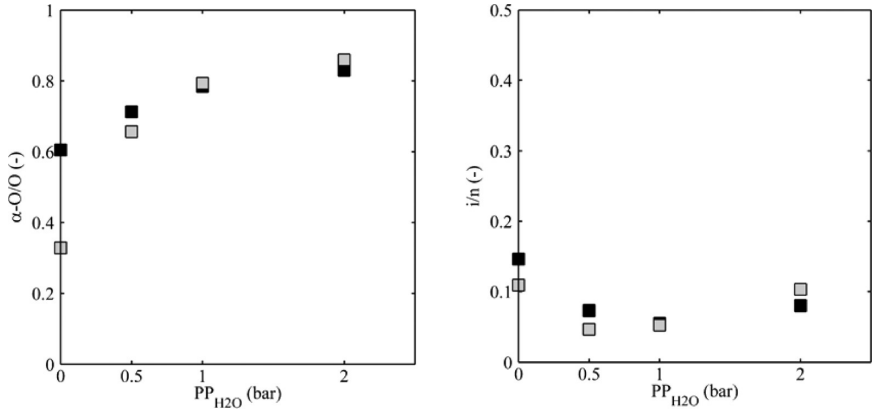

Figure 8. Fraction of α-olefins in the total fraction of linear olefinic product for the representative C_7 fraction (left) and ratio of branched to linear hydrocarbon contents for the representative C_5 fraction (right) as a function of water partial pressure for catalyst A (black squares) and catalyst B (gray squares).

olefin reactions. Alternatively, the higher CO partial pressures in our former study suppressed secondary olefin hydrogenation.[31]

Besides the hydrogenation and incorporation into a growing hydrocarbon chain, re-adsorbed α-olefins can undergo a double-bond shift reaction yielding internal olefins. This reaction has been shown to occur on metal sites in the presence of hydrogen as well as on solid acidic sites.[32] Whereas the total olefin content in catalyst A is not affected by the water addition, the fraction of internal olefins, here representatively shown by the content of α-heptene in the fraction of linear C_7 olefins, clearly increases by approximately 30% (see Figure 8, left). Even more pronounced is the effect in the case of catalyst B, where an increase from 35 to >80 mol % was observed. Again, smaller crystallites seem to facilitate significantly more secondary reactions either due to their intrinsic higher surface area or due to the different nature and composition of the surface (higher concentration of kink and edge sites). Only small amounts of water are sufficient to cloud/compensate this crystallite size effect. Water inhibits the described secondary reactions, which might occur not only on active sites relevant for chain growth but also on non-FT sites responsible for hydrogenation and isomerization reactions only.[29b,33]

A last type of secondary α-olefin reactions involves the formation of branched hydrocarbons. This mechanism developed by Schulz and co-workers and evidenced via co-feeding experiments[34] is not the sole proposed route to branched products. A primary pathway, based on the reaction of a surface alkylidene and a surface methyl species, has also been proposed.[35] It is often argued that steric hindrance on the densely populated catalyst surfaces result in the generally low yield of branched compounds. In the presented study a possible decrease in branching with the addition of water can be observed (see Figure 8, right). Due to the low overall concentrations, the observed trend needs to be viewed with caution. Nevertheless, it indicates that indeed a secondary mechanism, via the re-adsorption sites for α-olefins, to branched hydrocarbons could be present. Interestingly, both catalysts are affected to the same extent.

3.2.3. Spent Catalyst. Although the catalysts were studied in situ with X-ray diffractometry, the spent and subsequently passivated catalysts were studied under TEM. Although it was not possible to distinguish between the different cobalt oxidation states present, observed crystallite sizes correlate well with the calculated values from the XRD measurements. In addition, a subtle change of the support morphology was observed. In some sections of the observed spent catalysts, needle-like configurations of potential alumina phases were observed (see Figure 9). These possibly indicate the formation of an AlO(OH) phase Boehmite.[36] The presence of this phase could not be confirmed from the diffraction pattern, most likely due to its low concentration. Effects on catalyst activity and/or selectivity could also not be determined.

dx.doi.org/10.1021/cs500936t | ACS Catal. 2015, 5, 113−121

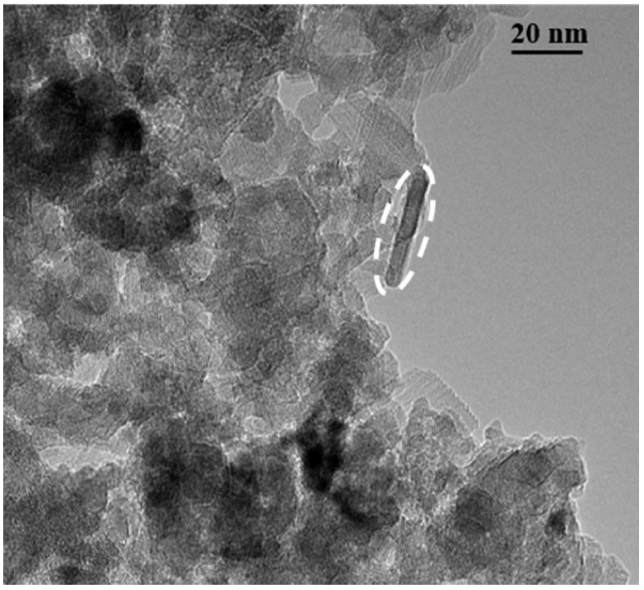

Figure 9. Representative TEM micrograph of alumina support of spent catalyst B with highlighted needle-like structure not observed prior to exposure to FT conditions.

4. CONCLUSION

Using two model catalyst systems with well-defined crystallite sizes, we could show that besides the previously reported tendency to undergo oxidation,[9] the presence of water, that is, a simulated high conversion condition, has a severe crystallite size dependent impact on the selectivity of cobalt-based catalytic systems in the Fischer–Tropsch synthesis. We could also shed light on the previously contradictory reports of the effect of water on the Fischer–Tropsch activity.[6,20] An increased water partial pressure results in not only a significantly increased surface specific activity but also an increased chain growth and lower methane and higher C_{5+} selectivity. Both effects are more pronounced for the smaller crystallites. The opposing effect of the oxidation of smaller crystallites under the oxidative stress of water could result in an overall stagnation or even deactivation as previously reported.[20] At high water partial pressures the selectivity to desired products (long-chained hydrocarbons at a low methane selectivity) over the smaller crystallites actually surpasses those of larger ones, contradicting previous studies on crystallite size dependency, most of which were carried out at rather water lean conditions.[4a−c,f,25a,26] Secondary olefin reactions, the hydrogenation to paraffins as well as the double-bond isomerization resulting in the formation of internal olefins, are more pronounced under dry conditions in the case of smaller crystallites. This class of reactions might be supported by active sites independent of the Fischer–Tropsch chain growth ensemble, which seem to be more prevalent on the small crystallites. However, only a small amount of water vapor seems to be sufficient to nearly selectively suppress their activity.

AUTHOR INFORMATION

Corresponding Author

*(M.C.) E-mail: Michael.Claeys@uct.ac.za.

Notes

The authors declare no competing financial interest.

REFERENCES

(1) Gallei, E. F.; Hesse, M.; Schwab, E. Development of Industrial Catalysts. In *Handbook of Heterogeneous Catalysis*; Wiley-VCH Verlag: Weinheim, Germany, 2008.
(2) Boudart, M.; McDonald, M. A. *J. Phys. Chem.* **1984**, *88*, 2185–2195.
(3) Haruta, M. *Catal. Today* **1997**, *36*, 153–166.
(4) (a) Fischer, N.; van Steen, E.; Claeys, M. *J. Catal.* **2013**, *299*, 67–80. (b) Bezemer, G. L.; Bitter, J. H.; Kuipers Herman, P. C. E.; Oosterbeek, H.; Holewijn, J. E.; Xu, X.; Kapteijn, F.; van Dillen, A. J.; de Jong, K. P. *J. Am. Chem. Soc.* **2006**, *128*, 3956–3964. (c) den Breejen, J. P.; Radstake, P. B.; Bezemer, G. L.; Bitter, J. H.; Froseth, V.; Holmen, A.; Jong, K. P. d. *J. Am. Chem. Soc.* **2009**, *131*, 7197–7203. (d) Welker, C. A. *Ruthenium based Fischer–Tropsch Synthesis on Crystallites and Clusters of Different Sizes*. Ph.D. thesis, University of Cape Town, 2007. (e) Ojeda, M.; Rojas, S.; Boutonnet, M.; Pérez-Alonso, F. J.; Javier García-García, F.; Fierro, J. L. G. *Appl. Catal., A* **2004**, *274*, 33–41. (f) Prieto, G.; Martínez, A.; Concepción, P.; Moreno-Tost, R. *J. Catal.* **2009**, *266*, 129–144. (g) Ho, S. W.; Houalla, M.; Hercules, D. M. *J. Phys. Chem.* **1990**, *94*, 6396–6399. (h) Reuel, R. C.; Bartholomew, C. H. *J. Catal.* **1984**, *85*, 78–88.
(5) Bezemer, G. L.; Remans, T. J.; van, B. A. P.; Dugulan, A. I. *J. Am. Chem. Soc.* **2010**, *132*, 8540–8541.
(6) (a) Bertole, C. J.; Mims, C. A.; Kiss, G. *J. Catal.* **2002**, *210*, 84–96. (b) Lögdberg, S.; Boutonnet, M.; Walmsley, J. C.; Järås, S.; Holmen, A.; Blekkan, E. A. *Appl. Catal., A* **2011**, *393*, 109–121. (c) Storsæter, S.; Borg, Ø.; Blekkan, E. A.; Holmen, A. *J. Catal.* **2005**, *231*, 405–419. (d) Claeys, M.; van Steen, E. *Catal. Today* **2002**, *71*, 419–427. (e) Schulz, H.; vein Steen, E.; Claeys, M. *Stud. Surf. Sci. Catal.* **1994**, *81*, 455–460 DOI: 10.1016/S0167-2991(08)63911-7. (f) van Steen, E.; Schulz, H. *Appl. Catal., A* **1999**, *186*, 309–320.
(7) Schulz, H.; Claeys, M.; Harms, S. *Stud. Surf. Sci. Catal.* **1997**, *107*, 193–200 DOI: 10.1016/S0167-2991(97)80334-5.
(8) Dry, M. E. *Catal. Today* **2002**, *71*, 227–241.
(9) Fischer, N.; Clapham, B.; Feltes, T.; van Steen, E.; Claeys, M. *Angew. Chem., Int. Ed.* **2014**, *53*, 1342–1345.
(10) Yates, I. C.; Satterfield, C. N. *Energy Fuels* **1991**, *5*, 168–173.
(11) Claeys, M.; Fischer, N. U.S Patent 8,597,598, 2013.
(12) Fischer, N.; van Steen, E.; Claeys, M. *Catal. Today* **2011**, *171*, 174–179.
(13) van Steen, E.; Claeys, M.; Dry, M. E.; Van de Loosdrecht, J.; Viljoen, E. L.; Visagie, J. L. *J. Phys. Chem. B* **2005**, *109*, 3575–3577.
(14) Schulz, H.; Boehringer, W.; Kohl, C.; Rahman, N.; Will, A. *DGMK Forschungsbericht* **1984**, *3*, 320–329.
(15) Fischer, N.; Minnermann, M.; Bäumer, M.; van Steen, E.; Claeys, M. *Catal. Lett.* **2012**, *142*, 830–837.
(16) Nakhaei Pour, A.; Taheri, S. A.; Anahid, S.; Hatami, B.; Tavasoli, A. *J. Nat. Gas Sci. Eng.* **2014**, *18*, 104–111.
(17) (a) Iglesia, E. *Appl. Catal., A* **1997**, *161*, 59–78. (b) van de Loosdrecht, J.; Balzhinimaev, B.; Dalmon, J. A.; Niemantsverdriet, J. W.; Tsybulya, S. V.; Saib, A. M.; van Berge, P. J.; Visagie, J. L. *Catal. Today* **2007**, *123*, 293–302. (c) Swart, J. C. W. *A Theoretical View on Deactivation of Cobalt-Based Fischer–Tropsch Catalysts*. Ph.D. thesis, University of Cape Town, 2008.
(18) (a) Li, J.; Zhan, X.; Zhang, Y.; Jacobs, G.; Das, T.; Davis, B. H. *Appl. Catal., A* **2002**, *228*, 203–212. (b) Jacobs, G.; Patterson, P. M.; Das, T. K.; Luo, M.; Davis, B. H. *Appl. Catal., A* **2004**, *270*, 65–76. (c) Li, J.; Jacobs, G.; Das, T.; Zhang, Y.; Davis, B. *Appl. Catal., A* **2002**, *236*, 67–76. (d) Jacobs, G.; Das, T. K.; Patterson, P. M.; Li, J.; Sanchez, L.; Davis, B. H. *Appl. Catal., A* **2003**, *247*, 335–343. (e) Jermwongratanachai, T.; Jacobs, G.; Shafer, W.; Ma, W.; Pendyala, V.; Davis, B.; Kitiyanan, B.; Khalid, S.; Cronauer, D.; Kropf, A. J.; Marshall, C. *Top. Catal.* **2014**, *57*, 479–490.
(19) Bezemer, G. L.; Radstake, P. B.; Koot, V.; van Dillen, A. J.; Geus, J. W.; de Jong, K. P. *J. Catal.* **2006**, *237*, 291–302.
(20) Hilmen, A. M.; Schanke, D.; Hanssen, K. F.; Holmen, A. *Appl. Catal., A* **1999**, *186*, 169–188.
(21) (a) van Santen, R. A.; Ghouri, M.; Hensen, E. M. J. *Phys. Chem. Chem. Phys.* **2014**, *16*, 10041–10058. (b) van Santen, R. A.;

Markvoort, A. J.; Filot, I. A. W.; Ghouri, M. M.; Hensen, E. J. M. *Phys. Chem. Chem. Phys.* **2013**, *15*, 17038−17063. (c) van Santen, R. A.; Markvoort, A. J.; Ghouri, M. M.; Hilbers, P. A. J.; Hensen, E. J. M. *J. Phys. Chem. C* **2013**, *117*, 4488−4504.
(22) Hibbitts, D. D.; Loveless, B. T.; Neurock, M.; Iglesia, E. *Angew. Chem., Int. Ed.* **2013**, *52*, 12273−12278.
(23) Van Hardeveld, R.; Hartog, F. *Surf. Sci.* **1969**, *15*, 189−230.
(24) (a) Fischer, N.; van Steen, E.; Claeys, M. *ChemCatChem.* **2014**, *6*, 1707−1713. (b) Bezemer, L.*Cobalt supported on carbon nanofibres as catalysts for the Fischer−Tropsch synthesis*. Ph.D. thesis, University Ultrecht, 2006.
(25) (a) Cheang, V. *Effect of Crystallite Size and Water Partial Pressure on thr Activity and Selectivity of Low Temperature Iron-based Fischer−Tropsch Catalysts*. Ph.D. thesis, University of Cape Town, 2009. (b) Mabaso, E. I.; van Steen, E.; Claeys, M. *DGMK/SCI-Conference "Synthesis Gas Chemistry"*; DGMK-Tagungsbericht, 2006; pp 93−100 (c) Carballo, J. M. G.; Yang, J.; Holmen, A.; García-Rodríguez, S.; Rojas, S.; Ojeda, M.; Fierro, J. L. G. *J. Catal.* **2011**, *284*, 102−108. (d) Welker, C.; Moss, J. R.; van Steen, E.; Claeys, M. *DGMK/SCI-Conference "Synthesis Gas Chemistry"*; DGMK-Tagungsbericht, 2006; pp 223−230 (e) Kang, J.; Deng, W.; Zhang, Q.; Wang, Y. *J. Energy Chem.* **2013**, *22*, 321−328.
(26) Mabaso, E. I. *Nanosized Iron Crystallites for Fischer−Tropsch Synthesis*. Ph.D. thesis, University of Cape Town, 2005.
(27) Claeys, M.; van Steen, E. *Surf. Sci. Catal.* **2004**, *152*, 601−680 DOI: 10.1016/S0167-2991(04)80465-8.
(28) (a) Iglesia, E.; Reyes, S. C.; Madon, R. J. *J. Catal.* **1991**, *129*, 238−256. (b) Madon, R. J.; Reyes, S. C.; Iglesia, E. *J. Phys. Chem.* **1991**, *95*, 7795−7804. (c) Gaube, J.; Klein, H. F. *J. Mol. Catal. A* **2008**, *283*, 60−68. (d) Gökcebay, H.; Schulz, H. EP Patent 0,071,770, 1983. (e) Schulz, H. *Top. Catal* **2003**, *26*, 73−85. (f) Schulz, H.; Roesch, S.; Gökcebay, H. *Selectivity of the Fischer−Tropsch Synthesis*; Verlag Glueckauf: Essen, Germany, 1981; pp 522−529.
(29) (a) Schulz, H.; Beck, K.; Erich, E. The Fischer-Tropsch carbon monoxide-hydrogenation, a nontrivial surface polymerization selectivity of chain branching. In *Proceedings of the 9th International Congress on Catalysis, Calgary*; Chemical Institute of Canada: Ottawa, Canada, 1988; Vol. 2. (b) Schulz, H.; Claeys, M. *Appl. Catal., A* **1999**, *186*, 71−90.
(30) Kuipers, E. W.; Scheper, C.; Wilson, J. H.; Vinkenburg, I. H.; Oosterbeek, H. *J. Catal.* **1996**, *158*, 288−300.
(31) Schulz, H.; van, S. E.; Claeys, M. *Top. Catal.* **1995**, *2*, 223−34.
(32) Germain, J. E.*Catalytic Conversion of Hydrocarbons*; Academic: New York, 1969; pp 322.
(33) Schulz, H.; Claeys, M. *Appl. Catal., A* **1999**, *186*, 91−107.
(34) (a) Schulz, H.; Beck, K.; Erich, E. *Chem. Inst. Can.* **1988**, 829−836. (b) Schulz, H.; Erich, E.; Gorre, H.; Van, S. E. *Catal. Lett.* **1990**, *7*, 157−167. (c) Schulz, H.; Rao, B. R.; Elstner, M. *Erdoel und Kohle* **1970**, *23*, 651−655.
(35) Lee, C. B.; Anderson, R. B.*Chain Grown in the Fischer−Tropsch Synthesis*; Verlag Chemie: Weinheim, Germany, 1985; pp II15−II22.
(36) Tsakoumis, N. E.; Rønning, M.; Borg, Ø.; Rytter, E.; Holmen, A. *Catal. Today* **2010**, *154*, 162−182.